Effect of Heterometal-Functionalization and Template Exchange on the Redox Chemistry of Molecular Vanadium Oxides

Simon Greiner,[a, b] Benjamin Schwarz,[a] Carsten Streb,*[a, b] and Montaha Anjass*[a, b]

Abstract: Polyoxometalates (POMs) have emerged as material of interest in many applications such as energy storage and conversion due to their redox activity and molecularly defined structure. However, especially for polyoxovanadates a lack of understanding between structural modifications and physicochemical properties remains. The present study leverages a lacunary dodecavanadate to systematically investigate the electronic effect of heterometal functionalization. While structural distortion affects the stability of the cluster, the redox potentials correlate with the overall cluster charge. Furthermore, we report the first bromide-templated analogue of this cluster family. While the halide anion is crucial for the formation of the cluster, no major effect on the electrochemical properties is observed. By improving the understanding of structure-property relationship in this work, we hope to enable a more predictable tuning of redox-properties of polyoxovandates.

Introduction

Metal oxides are state-of-the-art materials in important technological applications such as energy storage and conversion.[1,2] However, their controlled and predictable synthesis and rational redox-tuning remain challenging. Therefore, model systems are required to understand the structure-property relationship and derive rational approaches to manipulate physicochemical properties.[3]

Molecular metal oxides, so-called polyoxometalates (POMs), can be regarded as molecular analogues of solid-state oxides and therefore act as such model systems.[4] POMs are anionic metal oxo clusters, formed by self-assembly in solution. They consist of high-valent, early transition metals (often W, Mo, V).[5] Due to their versatile structure and rich redox-chemistry, they have been employed in various technological applications such as energy storage and conversion,[6,7] redox catalysis[8–10] and molecular electronics.[11]

For molybdenum- and tungsten-based POMs, the manipulation of electrochemical properties has been widely investigated.[6,12] Due to the molecular structure, the targeted manipulation by introduction of heterometals, template-exchange, counter-cations and pH can be separately studied.[6,12] Most studies concentrate on Keggin- and Dawson-type clusters, which can be synthesized with various tetrahedral templates and enable the introduction of heterometals into the metal-oxide-framework via lacunary binding sites.[13] However, similar studies remain scarce for polyoxovanadates (POVs)[14–17] as systematic access to heterometal-functionalized compounds is still challenging.[16,18,19] Only recently, studies provided more insights into functionalization with heterometals,[18,20–22] organic substituents[23,24] and counter cations.[25]

Recently, Matson and co-workers developed a systematic access route to metal-functionalized Lindqvist-type POV-alkoxides.[26,27] Exchange of a vanadium atom with d^0 heterometallic dopants (*e.g.* Ti^{4+}) shifts the vanadium-based redox processes to higher potentials.[27] Similarly, cathodic shifts were reported for electron rich replacements (*e.g.* Fe^{3+}).[28] Based on these results, rational optimizations towards the application of the POV as electron reservoirs in non-aqueous redox-flow batteries becomes possible.[21,29]

Over the last years, our group has established a platform for the controlled manipulation of a dodecavanadate cluster $(H_2NMe_2)_2[V_{12}O_{32}Cl]^{3-}$ (= **{V$_{12}$}**) by a so-called placeholder-cation approach.[30] Targeted substitution of the organic dimethyl ammonium placeholder cation in **{V$_{12}$}** gives access to a family of (transition-)metal-functionalized clusters. Functionalization of one or both binding sites with s-, d- and f-block metal cations has been reported.[20,30–35] Thereby the tuning of magnetic, electrochemical and (photo-) catalytic properties becomes possible.

Initial studies on the electrochemical properties focused on the functionalization with transition metals (Mn^{2+} and Fe^{3+}); both functionalizations led to the introduction of additional, transition-metal based redox-processes.[20,33,36,37] Very recent

[a] S. Greiner, Dr. B. Schwarz, Prof. Dr. C. Streb, Dr. M. Anjass
Institute of Inorganic Chemistry I
Ulm University
Albert-Einstein-Allee 11, 89081 Ulm (Germany)
E-mail: carsten.streb@uni-ulm.de
montaha.anjass@uni-ulm.de
[b] S. Greiner, Prof. Dr. C. Streb, Dr. M. Anjass
Helmholtz Institute Ulm (HIU)
Helmholtzstraße 11, 89081 Ulm (Germany)

Supporting information for this article is available on the WWW under https://doi.org/10.1002/chem.202102352

studies expanded these results to demonstrate that introduction of redox-inactive calcium ions results in a significant enhancement of the vanadate-based redox-activity.[35] The reduced states of $(n\mathrm{Bu_4N})_2[\mathrm{Ca^{II}}_2\mathrm{V_{12}O_{32}Cl(DMF)_3}]\cdot\mathrm{DMF}$ (= **{Ca$_2$V$_{12}$Cl}**, DMF = *N,N*-dimethyl formamide) were electrostatically and structurally stabilized by the Ca^{2+} ions, so that **{Ca$_2$V$_{12}$Cl}** showed five quasi-reversible redox-processes, while the non-functionalized **{V$_{12}$}** parent compound only showed one quasi-reversible redox-transition.

Herein, we build on these results and investigate the influence of the heterometal on the redox activity of the dodecavanadate cluster. By systematic variation of the heterometal, we compare the electrochemical properties and the molecular structure of **{Ca$_2$V$_{12}$Cl}** with similar, recently reported, analogues functionalized with strontium, manganese and cerium. Additionally, we report the first bromide-templated analogue of this cluster family and compare how chloride vs. bromide template affect the structural and electrochemical properties.

Results and Discussion

Characterization and structural comparison

To investigate the influence of heterometal-ions on the redox-properties of the **{V$_{12}$}** platform, we used the following literature-known di-metal-functionalized **{V$_{12}$}** species: **{Ca$_2$V$_{12}$Cl}**,[35] $(n\mathrm{Bu_4N})_2[\mathrm{Sr^{II}}_2(\mathrm{NMP})_3\mathrm{V_{12}O_{32}Cl}]\cdot\mathrm{NMP}\cdot\mathrm{acetone}$ (= **{Sr$_2$V$_{12}$}**, NMP = *N*-methyl-2-pyrrolidone),[32] $[\mathrm{Ce^{III}}_2(\mathrm{NMP})_8\mathrm{V_{12}O_{32}Cl}]\cdot\mathrm{NMP}\cdot\mathrm{acetone}$ (= **{Ce$_2$V$_{12}$}**)[31] and $(n\mathrm{Bu_4N})_4[\mathrm{Mn^{II}}_2\mathrm{V_{12}O_{32}Cl_3}]\cdot\mathrm{CH_3CN}$ (= **{Mn$_2$V$_{12}$}**, see Table 1).[20]

The clusters were selected based on the systematic variation of metal cation charge and ionic radius. While calcium and strontium have very similar electronic structures, strontium (135 pm) shows a larger ionic radius than calcium (120 pm) and consequently lower charge density. In contrast, cerium has an ionic radius (128 pm) between calcium and strontium; however, the threefold positive charge leads to higher charge density. Additionally, cerium exhibits f-orbitals, which could further influence the electronic structure and thus redox properties of the cluster. Meanwhile, manganese shows a significantly smaller ionic radius (89 pm) in comparison to calcium, leading to higher charge density. Additionally, manganese has partially occupied d-orbitals. The compounds' identity and purity were confirmed by elemental analysis, IR- and UV-Vis-spectroscopy, thermogravimetric analysis, and single-crystal X-ray diffraction.

As-prepared, all clusters are one-electron reduced species featuring one V^{4+} center, as reported in literature and indicated by the intervalence charge transfer band at *ca.* 980 nm in the UV-Vis-spectra (see Supporting Information, Figure S2). Earlier reports suggested that this reduction is necessary for the introduction of the second heterometal. While this holds true for compounds investigated here, we recently reported a fully oxidized di-potassium-functionalized **{V$_{12}$}** compound $[\mathrm{K_5(CH_3CN)_3V_{12}O_{32}Cl}]$ which demonstrates that the presence of reduced V^{4+} centers is not necessary for **{V$_{12}$}** di-functionalization.[38] We speculate, that the lower charge density of potassium enables the functionalization with more than one heterometal without the need for vanadium reduction. Since multiple potassium ions coordinate to the **{V$_{12}$}** cluster outside of the actual metal binding site, we have opted to not include it in this study.

Structural analysis of the metal binding site shows that with increasing charge-density, the distortion of the vanadate shell increases, as observed from the O-O-O-angle α (see Figure 1 and Supporting Information, Table S3). Upon metal coordination, α decreases from ca. 91° in **{V$_{12}$}** to 80° in **{Ca$_2$V$_{12}$Cl}** and 73° in **{Mn$_2$V$_{12}$}**. Metal binding therefore triggers a pincer-like movement of the vanadate shell, where the distance between the non-binding oxo-ligands of the hexagonal binding site increases (Figure 1, label "a"), while the distances between the coordinating oxo-ligands decreases (Figure 1, label "b"). While the distortion of the vanadate shell for Ce^{3+} and Mn^{2+} is comparable to values observed for mono-transition-metal-functionalized clusters (*e.g.* Co^{2+}),[30] less distortion is observed for Ca^{2+}. The least distortion is observed for the Sr^{2+}-ion, which has the lowest charge density of the metal ions investigated here.

To investigate the influence of the heterometal functionalization on the electrochemical properties, cyclic voltammograms (CVs) of the compounds were recorded in anhydrous, de-aerated DMF containing 0.1 M $(n\mathrm{Bu_4N})\mathrm{PF_6}$ as supporting electrolyte (all data referenced against Fc^+/Fc, see Figure 2). To increase comparability between the clusters with a different number of processes in anodic and cathodic direction, the processes are named counting from the open-circuit potential (OCP). Accordingly, R1 describes the first redox process in reductive direction. Respectively, O1 describes the first redox process in oxidative direction. For **{V$_{12}$}** and **{Ca$_2$V$_{12}$Cl}**, as recently reported by us,[35] the CV shows one and five (quasi-)

Table 1. Overview of the investigated compounds, oxidation state of and ligand at the introduced heterometal, template and overall cluster charge.

Abbreviation	Formula[a]	Heterometal [Oxidation state]	Template	Ligand[a]	Cluster charge	Ref.
{V$_{12}$}	$(n\mathrm{Bu_4N})_3[(\mathrm{H_2NMe_2})_2\mathrm{V_{12}O_{32}Cl}]$	n/a	Cl^-	n/a	3-	[30]
{Ca$_2$V$_{12}$Cl}	$(n\mathrm{Bu_4N})_2[\mathrm{Ca_2(DMF)_3V_{12}O_{32}Cl}]\cdot\mathrm{DMF}$	Ca [+2]	Cl^-	DMF	2-	[35]
{Sr$_2$V$_{12}$}	$(n\mathrm{Bu_4N})_2[\mathrm{Sr_2(NMP)_3V_{12}O_{32}Cl}]\cdot\mathrm{NMP\cdot acetone}$	Sr [+2]	Cl^-	NMP	2-	[32]
{Ce$_2$V$_{12}$}	$[\mathrm{Ce_2(NMP)_8V_{12}O_{32}Cl}]\cdot\mathrm{NMP\cdot acetone}$	Ce [+3]	Cl^-	NMP	0	[31]
{Mn$_2$V$_{12}$}	$(n\mathrm{Bu_4N})_4[\mathrm{Mn_2V_{12}O_{32}Cl_3}]\cdot\mathrm{MeCN}$	Mn [+2]	Cl^-	Cl^-	4-	[20]
{Ca$_2$V$_{12}$Br}	$(n\mathrm{Bu_4N})_2[\mathrm{Ca_2(DMF)_3V_{12}O_{32}Br}]\cdot\mathrm{DMF}$	Ca [+2]	Br^-	DMF	2-	This work

[a] DMF = *N,N*-dimethyl formamide; NMP = *N*-methyl-2-pyrrolidone.

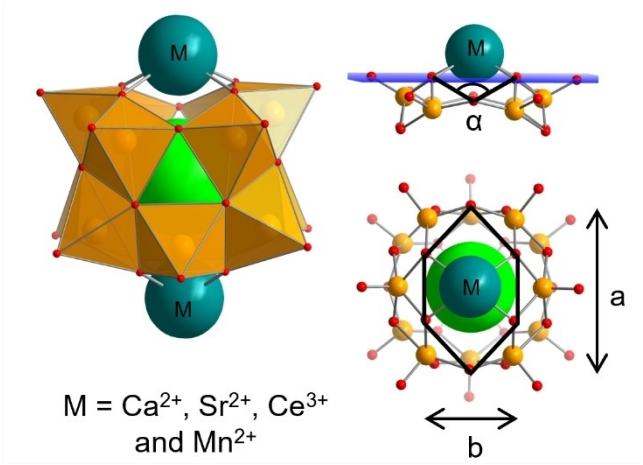

Figure 1. Left: Polyhedral representation of $\{M_2V_{12}\}$ with M = Ca^{2+}, Sr^{2+}, Ce^{3+} and Mn^{2+}. **Right**: Illustration of the metal binding site, highlighting the distortion angle α and the distance between the oxygen-plane and the metal ion (top) and the oxygen distances a and b (bottom). Color scheme: V and $[VO_5]$ polyhedral: yellow; O: red; Heterometal: teal; Cl: light green.

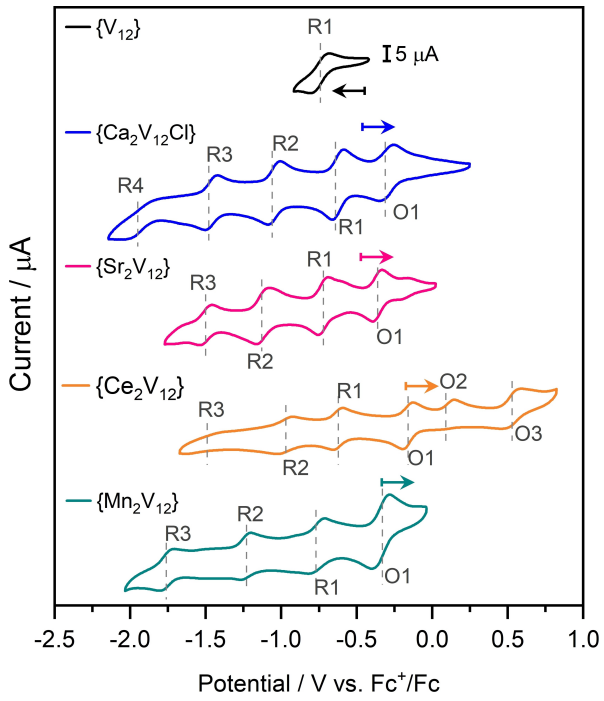

Figure 2. Cyclic voltammograms of $\{V_{12}\}$ (black), $\{Ca_2V_{12}Cl\}$ (blue), $\{Sr_2V_{12}\}$ (pink, $\{Ce_2V_{12}\}$ (orange) and $\{Mn_2V_{12}\}$ (teal). Conditions: Anhydrous, de-oxygenated DMF containing 0.1 M $(nBu_4N)PF_6$ as supporting electrolyte; Scan rate: 0.1 $V s^{-1}$; [cluster] = 1 mM.

reversible, one-electron redox processes, respectively. The OCP measurement indicates a fully oxidized cluster for $\{V_{12}\}$ and one electron reduced $\{Ca_2V_{12}Cl\}$, which is in line with earlier reports[30,35] and the IVCT-band observed in UV-Vis spectra (see Supporting Information, Figure S2).

Electrochemical analysis of $\{Sr_2V_{12}\}$

For $\{Sr_2V_{12}\}$, the CV shows four (quasi-) reversible redox processes between 0.0 and −2.0 V ($E_{1/2,O1}$ = −0.36, $E_{1/2,R1}$ = −0.72, $E_{1/2,R2}$ = −1.13 and $E_{1/2,R3}$ = −1.50 V). Scan-rate-dependent CV analysis (between 0.01 and 2.0 $V s^{-1}$, see Supporting Information, section 9a) revealed a linear relationship between the peak current and the square-root of the scan rate for all four processes, as expected by the Randles-Sevcik equation for reversible, diffusion-controlled processes. Due to the increase of the peak separation with higher scan rate, all four processes were assigned as quasi-reversible. Small shoulders can be observed for O1 and R1, which were assigned to the presence of trace amounts of protons in solution.[39] This is supported by earlier studies, which reported the isolation of $\{Sr_2V_{12}\}$ as protonated species.[32]

While the peak current ratio remains close to unity for O1, R1 and R3, the ratio increases for R2 at higher scan rates. This can be explained by the broadening of the associated reduction peak, leading to lower peak currents. This indicates rather slow kinetics of the reduction.

Since Sr^{2+}-ions are redox-inactive in the potential range used, all four processes are assigned to individual $V^{5+/4+}$ transitions. Notably, this indicates small cathodic shifts of 50, 80, 70 and 20 mV with respect to the valent isoelectronic $\{Ca_2V_{12}Cl\}$ for O1, R1, R2 and R3, respectively. In contrast to $\{Ca_2V_{12}Cl\}$, no fifth reduction is observed for $\{Sr_2V_{12}\}$. In addition, this process is nearly irreversible for $\{Ca_2V_{12}Cl\}$. Thus, we suggest that the overall cluster charge becomes too negative after the reduction of R3 (5-) and further reduction leads to decomposition of the cluster.

Electrochemical analysis of $\{Ce_2V_{12}\}$

For $\{Ce_2V_{12}\}$, the CV shows a significant anodic shift of the OCP in comparison to $\{Ca_2V_{12}Cl\}$. In reductive direction, two (quasi-) reversible processes are observed ($E_{1/2,R1}$ = −0.62 V and $E_{1/2,R2}$ = −0.97 V). At lower potentials, another reduction ($E_{1/2,R3}$ = −1.49 V) with limited reversibility (indicated by low peak-current of the re-oxidation), is observed. In oxidative direction, one (quasi-) reversible process ($E_{1/2,O1}$ = −0.16 V) is followed by a process with limited reversibility indicated by low peak-current of the re-reduction ($E_{1/2,O2}$ = 0.09 V). At higher potentials ($E_{1/2,O3}$ = 0.53 V), another (quasi-) reversible process is observed. O1 is tentatively assigned to the $V^{5+/4+}$ transition, after which all vanadium centers are fully oxidized. Oxidation of Ce^{3+} to Ce^{4+} (tentatively assigned for O2 and O3) could then easily lead to the expulsion of cerium from the binding site. Notably, only two reversible processes in cathodic direction are observed in comparison to four and three for $\{Ca_2V_{12}Cl\}$ and $\{Sr_2V_{12}\}$, respectively. We speculate, that this is associated with the high positive charge of the cerium ion. After reduction of R2, the coulombic attraction between the negatively charged cluster shell and the threefold positive charged cerium ions leads to a deeper penetration of the cerium into the cluster shell which could lead to a destabilization of the compound.

Process O1, R1 and R2 are expected to be vanadium-based and were further analyzed by Randles-Sevcik analysis, which shows a linear dependency of the peak current with the square-root of the scan rate, indicating reversible, diffusion-controlled processes (see Supporting Information, section 9b). For process O1 and R1, only minor increase of the peak separation is observed, suggesting both processes are reversible. Additionally, the peak current ratios of both processes remain close to unity. Process R2 exhibits more pronounced increase of the peak separation and was assigned as a quasi-reversible process.

Electrochemical analysis of {Mn_2V_{12}}

Electrochemical studies of **{Mn_2V_{12}}** show OCP at -0.34 V and three (quasi-) reversible processes in reductive direction ($E_{1/2,R1}=-0.77$ V, $E_{1/2,R2}=-1.23$ V and $E_{1/2,R3}=-1.76$ V). In oxidative direction one (quasi-) reversible process ($E_{1/2,O1}=-0.34$ V) and two rather sluggish processes ($E_{1/2,O2}=-0.02$ V and $E_{1/2,O3}=0.50$ V) are observed, which have been assigned to Mn^{2+}/Mn^{3+} transition in earlier reports.[20]

Consequently, processes R1, R2, R3 and O1 are assigned to $V^{5+/4+}$ transitions and were further investigated by scan-rate-dependent analysis (see Supporting Information, section 9c). For process O1, the re-reduction shows a clear deviation from linearity when plotted against the square-root of the scan rate and increasing peak current ratios i_{ox}/i_{red} are observed. Both indicate limited reversibility. This is in line with initial structural considerations, which suggest that for highly distorted clusters, the presence of at least one reduced V^{4+} is required for stable di-functionalization. After oxidation O1, a di-functionalized but fully oxidized vanadate species is obtained, which is suggested to be less electrostatically stable and leads to lower reversibility (possibly due to heterometal expulsion). Process R1 shows a typical diffusion-controlled, (quasi-) reversible behavior. For process R2, splitting into three reductive peaks becomes apparent at higher scan rates. At the same time, the peak current ratio i_{ox}/i_{red} is increasing. We suggest that this unusual behavior is caused by a ligand exchange at the manganese ion.[40,41] After reduction of process R1, the cluster exhibits a high negative charge (5-). This can partially be compensated by exchange of the chloride ligands with neutral solvent molecules. This leads to three species where A) two chlorides (overall charge 3^-), B) one chloride (overall charge 4^-) and C) zero chlorides (overall charge 5^-) have been exchanged. Based on electrostatic considerations, we suggest that the cluster species with lower negative charge are reduced at less negative potentials. At low scan rates, we propose that only the fully exchanged species A) is observed. However, at higher scan rates, the exchange process is not complete, and reductions of all three species become observable. This is further supported by the increasing peak current ratio i_{ox}/i_{red} at higher scan rates. Increasing contribution of species B) and C) leads to a lower peak current for the initial peak (which is assigned to species A)). Since the re-oxidation remains as a single peak, the peak current ratio increases.[41]

Finally, process R3 shows a deviation from linearity for the re-oxidation in the Randles-Sevcik-plot and peak current ratio of ca. 0.5 at low scan rate. At higher scan rate, the peak current ratio becomes close to unity. This indicates that the cluster becomes unstable after reduction R3, which can be explained by the high negative charge of the cluster (7- without ligand exchange, 5- assuming exchange of both Cl^- with solvent ligands).

Comparison of the electrochemical properties

Comparison of the electrochemical properties of the five compounds concerning the structural distortions shows only minor contribution of the geometric values. Instead, a significant correlation between the anion charge and the redox potentials can be observed (see Figure 3). In all cases studied, increase of the anionic charge of the respective cluster leads to a cathodic shift of the redox-potentials. This is in line with observations in Keggin-type polyoxotungstates, where a similar linear relationship between cluster charge and redox potentials was reported.[6,12,42] While further investigations are necessary to understand the interaction between the heterometal and the vanadate shell, it is evident, that the incorporation of the heterometals increases the cluster stability upon reduction, leading to more accessible redox-processes.

Recent studies by Matson and co-workers[22] on metal-functionalized Lindqvist-type POV-alkoxide clusters suggested a correlation between the Lewis acidity of the metal center and the corresponding vanadium-based redox potentials. Positive potential shifts were reported upon substitution of a V^{4+} with more Lewis-acidic metal ions (based on aqueous $pK_a(M(H_2O)_n)$ values). A similar correlation cannot be observed here, as for example **{Sr_2V_{12}}** shows more positive potentials than **{$Ca_2V_{12}Cl$}** although Sr^{2+} ($pK_a=13.2$) shows lower Lewis-acidity compared with Ca^{2+} ($pK_a=12.6$).[43] Note however, that the present study investigates alkaline metal ions, whereas the Matson group used metal ions with higher Lewis acidity, for example Ti^{4+}.[22]

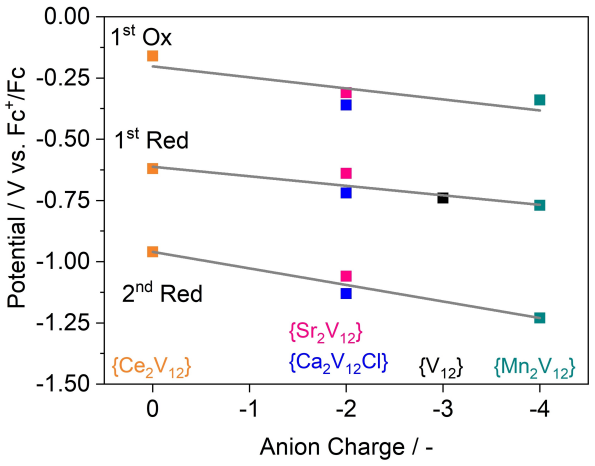

Figure 3. Dependence of the first oxidation, first reduction and second reduction potentials on the negative charge of the pristine cluster.

Additionally, previous studies on iron-substituted **{V_{12}}** and Lindqvist POVs have already shown marked differences in their electrochemical behavior and electronic structure.[28,33]

Synthesis and characterization of {$Ca_2V_{12}Br$}

In order to further explore the electrochemical tuneability of **{V_{12}}** we set out to investigate the influence of the template. Initial theoretical and experimental data showed that the chloride is essential for the assembly of the **{V_{12}}** framework but does not provide significant energetic stabilization for the final cluster.[30] In addition, structural analyses suggest that the **{V_{12}}** framework should be able to accommodate slightly larger templates such as bromide. To test this hypothesis, we modified the **{$Ca_2V_{12}Cl$}** synthesis and replaced chloride with bromide: To this end, (nBu$_4$N)$_3$[$H_3V_{10}O_{28}$] was reacted with $Ca(NO_3)_2\cdot 4\ H_2O$ and (nBu$_4$N)Br in DMF at 80 °C for 8 days, yielding (nBu$_4$N)$_2$[$Ca_2V_{12}O_{32}Br(DMF)_3$]·DMF (=**{$Ca_2V_{12}Br$}**). Diffusion of acetone into the reaction mixture gave single-crystalline materials suitable for X-ray diffraction (SC-XRD) (yield: 22% based on V).

SC-XRD analysis shows virtually the same structure and crystallographic dimensions as **{$Ca_2V_{12}Cl$}** (see Supporting Information, section 6). Briefly, the vanadate shell is formed around the central bromide template and both metal binding sites are occupied by calcium ions, which are coordinated to four bridging μ^3-oxo-ligands from one **{V_{12}}**. Additionally, each Ca^{2+} ion is coordinated by three μ^2-DMF ligands, which link to a Ca^{2+} ion of a neighboring cluster. Thereby, individual **{$Ca_2V_{12}Br$}** clusters are connected and form infinite 1D chains, which align co-parallel in the crystal lattice. The chains are separated by charge-balancing tetra-*n*-butyl ammonium cations and solvent DMF molecules. This is in line with the connectivity and 3D arrangement observed for the {$Ca_2V_{12}Cl$} compound. Full characterization by UV-Vis- and IR-spectroscopy, elemental analysis and thermogravimetric analysis unambiguously confirm the expected sum formula and cluster structure.

Structural analysis of the vanadate framework and the heterometal binding site of **{$Ca_2V_{12}Br$}** revealed virtually the same geometric values as observed for **{$Ca_2V_{12}Cl$}** and suggests that the exchange of the central anion does not influence the vanadate framework. We speculate, that the unsuccessful synthesis of fluoride- and iodide-templated **{V_{12}}** is based on the significantly smaller (F^-: 133 pm) and larger (I^-: 220 pm) ionic radii, while chloride (181 pm) and bromide (196 pm) are of similar size. Similar observations have been made for related POVs, where synthesis of bromide and chloride analogues was possible, but neither flouride nor iodide analogues could be synthesized.[44–46]

Electrochemical analysis of {$Ca_2V_{12}Br$}

Electrochemical studies were performed on **{$Ca_2V_{12}Br$}** in DMF (0.1 M (nBu$_4$N)PF_6 as supporting electrolyte; referenced against Fc^+/Fc) and compared with the **{$Ca_2V_{12}Cl$}** (see Figure 4). The

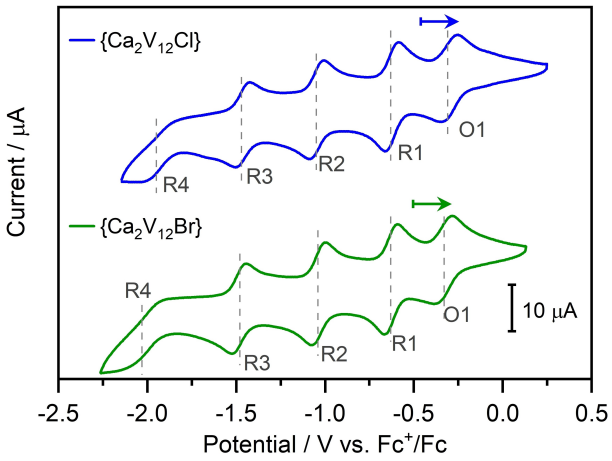

Figure 4. Cyclic voltammograms of **{$Ca_2V_{12}Cl$}** (blue) and **{$Ca_2V_{12}Br$}** (green). Conditions: Anhydrous, de-oxygenated DMF containing 0.1 M (nBu$_4$N)PF_6 as supporting electrolyte; Scan rate: 0.1 $V\,s^{-1}$; [cluster] = 1 mM.

voltammograms show five quasi-reversible redox processes (see Table 2). Scan-rate-dependent measurements show quasi-reversible, one electron processes for O1, R1, R2 and R3 (see Supporting Information, section 9d). The most negative process R4 is not fully reversible, as indicated by low peak current of the re-oxidation and large peak separation. Only minor shifts (< 20 mV) in the redox potentials in comparison with **{$Ca_2V_{12}Cl$}** are observed. This demonstrates that the central anion does not have significant effects on the redox-properties of the vanadium centers and indeed is mainly acting as template during synthesis.

Similar studies by Hayashi and co-workers[46] on a related $[V_{16}O_{38}X]^{4-}$ (=**{$V_{16}X$}**, with X = Cl^-, Br^-) showed marked geometric variations between the chloride and bromide species. The cluster size of the chloride analogue is smaller in comparison to the bromide analogue, indicating a stronger interaction between the template and the vanadium atoms.[46] While the reason for this is not understood, we speculate that this is associated with the less negative charge density on the vanadate shell in the {$V_{16}X$} cluster in comparison with the {V_{12}} cluster. Exchange of the template from chloride to bromide led to significantly larger anodic shifts of the first reduction wave (ca. 90 mV). The authors assigned this to the higher electron density of the cluster shell due to the smaller size. Additionally, the third reduction wave was less reversible for **{$V_{16}Br$}** in

Table 2. Half-wave potentials of the investigated compounds (referenced against Fc^+/Fc).

	$E_{1/2,O2}$ [V]	$E_{1/2,O1}$ [V]	$E_{1/2,R1}$ [V]	$E_{1/2,R2}$ [V]	$E_{1/2,R3}$ [V]	$E_{1/2,R4}$ [V]
{V_{12}}			−0.74			
{$Ca_2V_{12}Cl$}		−0.31	−0.64	−1.06	−1.48	−1.95[a]
{Sr_2V_{12}}		−0.36	−0.72	−1.13	−1.50	
{Ce_2V_{12}}	0.09[a]	−0.16	−0.62	−0.97	−1.49[a]	
{Mn_2V_{12}}	−0.02[a]	−0.34	−0.77	−1.23	−1.76	
{$Ca_2V_{12}Br$}		−0.33	−0.63	−1.04	−1.48	−2.03[a]

[a] Sluggish kinetics and/or limited reversibility.

comparison with the chloride analogue. This was assigned to repulsive interactions of the negative cluster shell with the larger bromide anion.

In a related study on $[(Bi(DMSO)_3)_2V_{12}O_{33}X]^-$ (= **{$Bi_2V_{12}X$}**, X = Cl^-, Br^-; DMSO = dimethyl sulfoxide), Streb and co-workers observed no significant structural effects of chloride vs. bromide templating.[47] However, the bromide species showed significantly higher photooxidative activity. This was attributed to the heavy atom effect of the bromide, leading to increased spin-orbit coupling and faster intersystem crossing to the reactive triplet state.

Our results are in line with observations with molybdenum- and tungsten-based POMs, where exchange of the template has insignificant effects for same valent templates. However, a clear correlation between the reduction potentials and the oxidation state of the template, and hence the charge of the cluster, is observed.[6,12]

Conclusions

In sum, we report a systematic study of the influence of heterometal substitution and template exchange on the electrochemical behavior of the dodecavanadate **{V_{12}}**. For the valence isoelectronic compounds **{$Ca_2V_{12}Cl$}** and **{Sr_2V_{12}}**, shifts of the redox potentials can be attributed to structural changes. Stronger distortions in comparison with the parent **{V_{12}}** lead to anodic shifts. However, the overall effect remains small (< 80 mV). To enable the di-functionalization with the small manganese ion, reduction of the **{V_{12}}** cluster shell seems crucial. This suggests that the reduction step is necessary to compensate for distortion of the vanadate shell upon functionalization. At the same time, a correlation between the overall cluster charge and the redox potentials is observed. Exchange of the central template anion from chloride to bromide shows no major effect on the electrochemical properties. By improving the understanding of the tuning parameters of POVs, we hope to gain more control over the electrochemical properties and highlight the potential of this material class for applications in (redox-)catalysis and electrochemical energy storage.

Experimental Section

Synthesis of {$Ca_2V_{12}Br$}

(nBu$_4$N)[$H_3V_{10}O_{28}$][48] (300 mg, 0.16 mmol, 1 eq.), $Ca(NO_3)\cdot 4\ H_2O$ (120 mg, 0.51 mmol, 3.3 eq.) and (nBu$_4$N)Br (80 mg, 0.25 mmol, 1.6 eq.) were dissolved in *N,N*-dimethyl formamide (10 ml) and stirred for 8 days at 80 °C. Diffusion of acetone into the reaction mixture at room temperature yielded dark green crystals suitable for X-ray diffraction. Yield: 86 mg (42 μmol, 22% based on V).

Crystallographic data for {$Ca_2V_{12}Br$}

$C_{44}H_{100}N_6O_{36}BrV_{12}Ca_2$, $M_w = 2060.64\ g\,mol^{-1}$, monoclinic, space group $P2_1/c$, $a = 10.7225(3)$ Å, $b = 29.3069(8)$ Å, $c = 28.3117(7)$ Å, $\beta = 95.4158(12)°$, $V = 8857.0(4)$ Å^3, $Z = 4$, μ(Mo K_α) = 1.844 mm^{-1}, 149832 reflections collected, 18199 unique which were used in all calculations; Structure solution and refinement was done using OLEX2.[49] Final $R1 = 0.0718$ and $wR2 = 0.1675$ (all data).

Deposition Number(s) 2075586 (for **{$Ca_2V_{12}Br$}**) contain(s) the supplementary crystallographic data for this paper. These data are provided free of charge by the joint Cambridge Crystallographic Data Centre and Fachinformationszentrum Karlsruhe Access Structures service.

Electrochemical characterization

Electrochemical measurements were performed on a Pine Research WaveDriver 200 equipped with a standard three-electrode arrangement: working electrode: glassy carbon electrode ($d = 3$ mm); Reference electrode: Ag wire (in a glass frit containing electrolyte solution); Counter electrode: Pt wire. All potentials are referenced against Fc^+/Fc. All experiments were performed in dry DMF using (nBu$_4$N)PF_6 (0.1 M) as supporting electrolyte. The solutions were purged with argon for at least 20 min prior to the experiments and kept under a slight positive argon pressure. Voltammograms were *iR* compensated at 95% as determined by electrochemical impedance spectroscopy within the Aftermath software.

Acknowledgements

Financial support by Ulm University, the Helmholtz-Gemeinschaft (HGF) and the Deutsche Forschungsgemeinschaft (STR1164/12, STR1164/14, DFG Cluster of Excellence EXC 2154, "POLiS", project no: 390874152; Collaborative Research Center TRR234 "CataLight", project no: 364549901) is gratefully acknowledged. S. G. gratefully acknowledges financial support through a PhD fellowship by the Fonds der Chemischen Industrie (FCI). M. A. acknowledges the State of Baden-Württemberg for a Margarete von Wrangell-fellowship. Dr. Dieter Sorsche is acknowledged for helpful discussions. This work contributes to the research performed in CELEST (the Center for Electrochemical Energy Storage Ulm-Karlsruhe) and the ERC Consolidator Grant project SupraVox (grant no: 101002212). Open access funding enabled and organized by Projekt DEAL.

Conflict of Interest

The authors declare no conflict of interest.

Keywords: electrochemistry · metal-functionalization metal oxides · polyoxometalate · self-assembly

[1] J. B. Goodenough, Y. Kim, *Chem. Mater.* **2010**, *22*, 587–603.
[2] A. Kudo, Y. Miseki, *Chem. Soc. Rev.* **2009**, *38*, 253–278.
[3] R. Schlögl, *Angew. Chem. Int. Ed.* **2011**, *50*, 6424–6426.
[4] A. Müller, S. Roy, *Coord. Chem. Rev.* **2003**, *245*, 153–166.
[5] D.-L. L. Long, R. Tsunashima, L. Cronin, *Angew. Chem. Int. Ed.* **2010**, *49*, 1736–1758; *Angew. Chem.* **2010**, *122*, 1780–1803.
[6] M. Sadakane, E. Steckhan, *Chem. Rev.* **1998**, *98*, 219–238.
[7] Y. Ji, L. Huang, J. Hu, C. Streb, Y.-F. Song, *Energy Environ. Sci.* **2015**, *8*, 776–789.

[8] Q. Yin, J. M. Tan, C. Besson, Y. V. Geletii, D. G. Musaev, A. E. Kuznetsov, Z. Luo, K. I. Hardcastle, C. L. Hill, *Science* **2010**, *328*, 342–345.
[9] C. Streb, *Dalton Trans.* **2012**, *41*, 1651.
[10] B. Rausch, M. D. Symes, G. Chisholm, L. Cronin, *Sci. J.* **2014**, *345*, 1326–1330.
[11] M. Stuckart, K. Y. Monakhov, *Chem. Sci.* **2019**, *10*, 4364–4376.
[12] T. Ueda, *ChemElectroChem* **2018**, *5*, 823–838.
[13] A. Kondinski, T. N. Parac-Vogt, *Front. Chem.* **2018**, *6*, 346.
[14] W. G. Klemperer, T. A. Marquart, O. M. Yaghi, *Angew. Chem. Int. Ed. Engl.* **1992**, *31*, 49–51; *Angew. Chem.* **1992**, *104*, 51–53.
[15] M. Anjass, G. A. Lowe, C. Streb, *Angew. Chem. Int. Ed.* **2021**, *60*, 7522–7532; *Angew. Chem.* **2021**, *133*, 7600–7611.
[16] Y. Hayashi, *Coord. Chem. Rev.* **2011**, *255*, 2270–2280.
[17] C. Streb, in *Polyoxometalate-Based Assemblies and Functional Materials, Structure and Bonding* (Ed. Y.-F. Song), Springer Cham, **2018**, pp. 31–47.
[18] K. Y. Monakhov, W. Bensch, P. Kögerler, *Chem. Soc. Rev.* **2015**, *44*, 8443–8483.
[19] J. Livage, *Coord. Chem. Rev.* **1998**, *178–180*, 999–1018.
[20] K. Kastner, J. Forster, H. Ida, G. N. Newton, H. Oshio, C. Streb, *Chem. Eur. J.* **2015**, *21*, 7686–7689.
[21] L. E. VanGelder, E. M. Matson, *J. Mater. Chem. A* **2018**, *6*, 13874–13882.
[22] R. L. Meyer, M. H. Anjass, B. E. Petel, W. W. Brennessel, C. Streb, E. M. Matson, *Chem. Eur. J.* **2020**.
[23] L. E. VanGelder, B. E. Petel, O. Nachtigall, G. Martinez, W. W. Brennessel, E. M. Matson, *ChemSusChem* **2018**, *11*, 4139–4149.
[24] O. Nachtigall, J. Spandl, *Chem. Eur. J.* **2018**, *24*, 2785–2789.
[25] E. Schreiber, N. A. Hartley, W. W. Brennessel, T. R. Cook, J. R. McKone, E. M. Matson, *ACS Appl. Mater. Interfaces* **2019**, *2*, 8985–8993.
[26] F. Li, L. E. VanGelder, W. W. Brennessel, E. M. Matson, *Inorg. Chem.* **2016**, *55*, 7332–7334.
[27] L. E. VanGelder, W. W. Brennessel, E. M. Matson, *Dalton Trans.* **2018**, *47*, 3698–3704.
[28] F. Li, S. H. Carpenter, R. F. Higgins, M. G. Hitt, W. W. Brennessel, M. G. Ferrier, S. K. Cary, J. S. Lezama-Pacheco, J. T. Wright, B. W. Stein, M. P. Shores, M. L. Neidig, S. A. Kozimor, E. M. Matson, *Inorg. Chem.* **2017**, *56*, 7065–7080.
[29] L. E. VanGelder, A. M. Kosswattaarachchi, P. L. Forrestel, T. R. Cook, E. M. Matson, *Chem. Sci.* **2018**, *9*, 1692–1699.
[30] K. Kastner, J. T. J. T. Margraf, T. Clark, C. Streb, *Chem. Eur. J.* **2014**, *20*, 12269–12273.
[31] A. Seliverstov, C. Streb, *Chem. Eur. J.* **2014**, *20*, 9733–9738.
[32] B. Schwarz, M. Dürr, K. Kastner, N. Heber, I. Ivanović-Burmazović, C. Streb, *Inorg. Chem.* **2019**, *58*, 11684–11688.
[33] M. H. Anjass, K. Kastner, F. Nägele, M. Ringenberg, J. F. Boas, J. Zhang, A. M. Bond, T. Jacob, C. Streb, *Angew. Chem. Int. Ed.* **2017**, *56*, 14749–14752; *Angew. Chem.* **2017**, *129*, 14944–14947.
[34] K. Kastner, M. Lechner, S. Weber, C. Streb, *ChemistrySelect* **2017**, *2*, 5542–5544.
[35] S. Greiner, B. Schwarz, M. Ringenberg, M. Dürr, I. Ivanovic-Burmazovic, M. Fichtner, M. Anjass, C. Streb, *Chem. Sci.* **2020**, *11*, 4450–4455.
[36] S. Sproules, *Angew. Chem. Int. Ed.* **2019**, *58*, 10043–10047.
[37] M. H. Anjass, K. Kastner, F. Nägele, M. Ringenberg, J. F. Boas, J. Zhang, A. Bond, T. Jacob, C. Streb, *Angew. Chem. Int. Ed.* **2019**, *58*, 10048–10050.
[38] S. Greiner, M. Anjass, C. Streb, *CrystEngComm* **2021**, 23, 3946–3950.
[39] B. Keita, L. Nadjo, *J. Electroanal. Chem. Interfacial Electrochem.* **1987**, *227*, 77–98.
[40] J. Friedl, R. Al-Oweini, M. Herpich, B. Keita, U. Kortz, U. Stimming, *Electrochim. Acta* **2014**, *141*, 357–366.
[41] D. Lexa, P. Rentien, J. M. Savéant, F. Xu, *J. Electroanal. Chem. Interfacial Electrochem.* **1985**, *191*, 253–279.
[42] J.-J. J. Chen, M. A. Barteau, *Ind. Eng. Chem. Res.* **2016**, *55*, 9857–9864.
[43] D. D. Perrin, *Ionisation Constants of Inorganic Acids and Bases in Aqueous Solution*, Pergamon, Oxford, U. K., **1982**.
[44] A. Müller, M. Penk, R. Rohlfing, E. Krickemeyer, J. Döring, *Angew. Chem. Int. Ed. Engl.* **1990**, *29*, 926–927; *Angew. Chem.* **1990**, *102*, 927–929.
[45] K. Okaya, T. Kobayashi, Y. Koyama, Y. Hayashi, K. Isobe, *Eur. J. Inorg. Chem.* **2009**, *2009*, 5156–5163.
[46] N. Kato, Y. Hayashi, *Dalton Trans.* **2013**, *42*, 11804–11811.
[47] J. Tucher, K. Peuntinger, J. T. Margraf, T. Clark, D. M. Guldi, C. Streb, *Chem. Eur. J.* **2015**, *21*, 8716–8719.
[48] W. G. Klemperer, in *Inorg. Synth. Vol. 27*, John Wiley & Sons, **1990**, p. 83.
[49] O. V. Dolomanov, L. J. Bourhis, R. J. Gildea, J. A. K. Howard, H. Puschmann, *J. Appl. Crystallogr.* **2009**, *42*, 339–341.

Manuscript received: June 30, 2021
Accepted manuscript online: July 19, 2021
Version of record online: August 6, 2021

